International Journal of Applied Earth Observation and Geoinformation 17 (2012) 43–54

Contents lists available at SciVerse ScienceDirect

International Journal of Applied Earth Observation and Geoinformation

journal homepage: www.elsevier.com/locate/jag

Improving land surface soil moisture and energy flux simulations over the Tibetan plateau by the assimilation of the microwave remote sensing data and the GCM output into a land surface model

Hui Lu[a,b,*], Toshio Koike[b], Kun Yang[c], Zeyong Hu[d], Xiangde Xu[e], Mohamed Rasmy[b], David Kuria[f], Katsunori Tamagawa[b]

[a] Ministry of Education Key Laboratory for Earth System Modeling, Center for Earth System Science, Institute for Global Change Studies, Tsinghua University, Beijing, 100084, China
[b] The Department of Civil Engineering, The University of Tokyo, Tokyo, 113-8658, Japan
[c] The Institute of Tibet Research, Chinese Academy of Science, Beijing, 100085, China
[d] The Institute of Cold and Arid Region Research, Chinese Academy of Science, Lanzhou, 730000, China
[e] Chinese Academy of Meteorology Science, Chinese Meteorological Administration, Beijing, 100081, China
[f] Department of Geomatic Engineering and Geospatial Information Systems, Jomo Kenyatta University of Agriculture and Technology, Nairobi, P.O. 62000-00200, Kenya

ARTICLE INFO

Article history:
Received 28 January 2011
Accepted 4 September 2011

Keywords:
Microwave remote sensing
Soil moisture
Surface energy flux
Data assimilation
Tibetan plateau

ABSTRACT

The land surface soil moisture is a crucial variable in weather and climate models. This study presents a land data assimilation system (LDAS) that aims to improve the simulation of the land surface soil moisture and energy fluxes by merging the microwave remote sensing data and the general circulation model (GCM) output into a land surface model (LSM). This system was applied over the Tibetan Plateau, using the National Centers for Environmental Prediction (NCEP) reanalysis data as forcing data and the Advanced Microwave Scanning Radiometers for EOS (AMSR-E) brightness temperatures as an observation. The performance of our four data sources, which were NCEP, AMSR-E, LDAS and simulations of Simple Biosphere Model 2 (SiB2), was assessed against 5 months of *in situ* measurements that were performed at two stations: Gaize and Naqu. For the surface soil moisture, the LDAS simulations were superior to both NCEP and SiB2, and there was more than a one-third reduction in the root mean squared errors (RMSE) for both of the stations. Compared with the AMSR-E soil moisture retrievals, the LDAS simulations were comparable at the Gaize station, and they were superior at the Naqu station. For the whole domain intercomparison, the results showed that the LDAS simulation of the soil moisture field was more realistic than the NCEP and SiB2 simulations and that the LDAS could estimate land surface states properly even in the regions where AMSR-E failed to cover and/or during the periods that the satellite did not overpass. For the surface energy fluxes, the LDAS estimated the latent heat flux with an acceptable accuracy (RMSE less than 35 W/m^2), with a one-third reduction in the RMSE from the SiB2. For the 5-month whole plateau simulation, the LDAS produced a much more reasonable Bowen Ratio than the NCEP, and it also generated a clear contrast of the land surface status over the plateau, which was wet in the southeast and dry in the northwest, during the monsoon and post-monsoon seasons. Because the LDAS only uses globally available data sets, this study reveals the potential of the LDAS to improving the land surface energy and water flux simulations in ungauged and/or poorly gauged regions.

1. Introduction

The soil moisture is an essential variable that governs the interactions between the land surface and the atmosphere (Betts et al., 1996; Entekhabi et al., 1996). The soil moisture controls the ratio of the runoff to infiltration (Delworth and Manabe, 1988; Wagner et al., 2003), controls the surface energy partition (Entekhabi et al., 1996; Prigent et al., 2005), and influences the development of vegetation and the carbon cycle. The soil moisture-precipitation feedback tendency has been identified by Koster et al. (2003), Koster (2004) and Pal and Eltahir (2002).

The soil moisture profile can be observed at a point scale using gravimetric methods or a Time Domain Reflectormetry (TDR). However, these point information are insufficient for research and applications at regional scales, and are not available in the remote regions that are difficult to access because building and maintaining such stations is costly and difficult. Conversely, satellite remote

* Corresponding author at: The Center for Earth System Science, Tsinghua University, Beijing 100084, China. Tel.: +86 10 62772565.
E-mail address: luhui@tsinghua.edu.cn (H. Lu).

0303-2434/$ – see front matter © 2011 Elsevier B.V. All rights reserved.
doi:10.1016/j.jag.2011.09.006

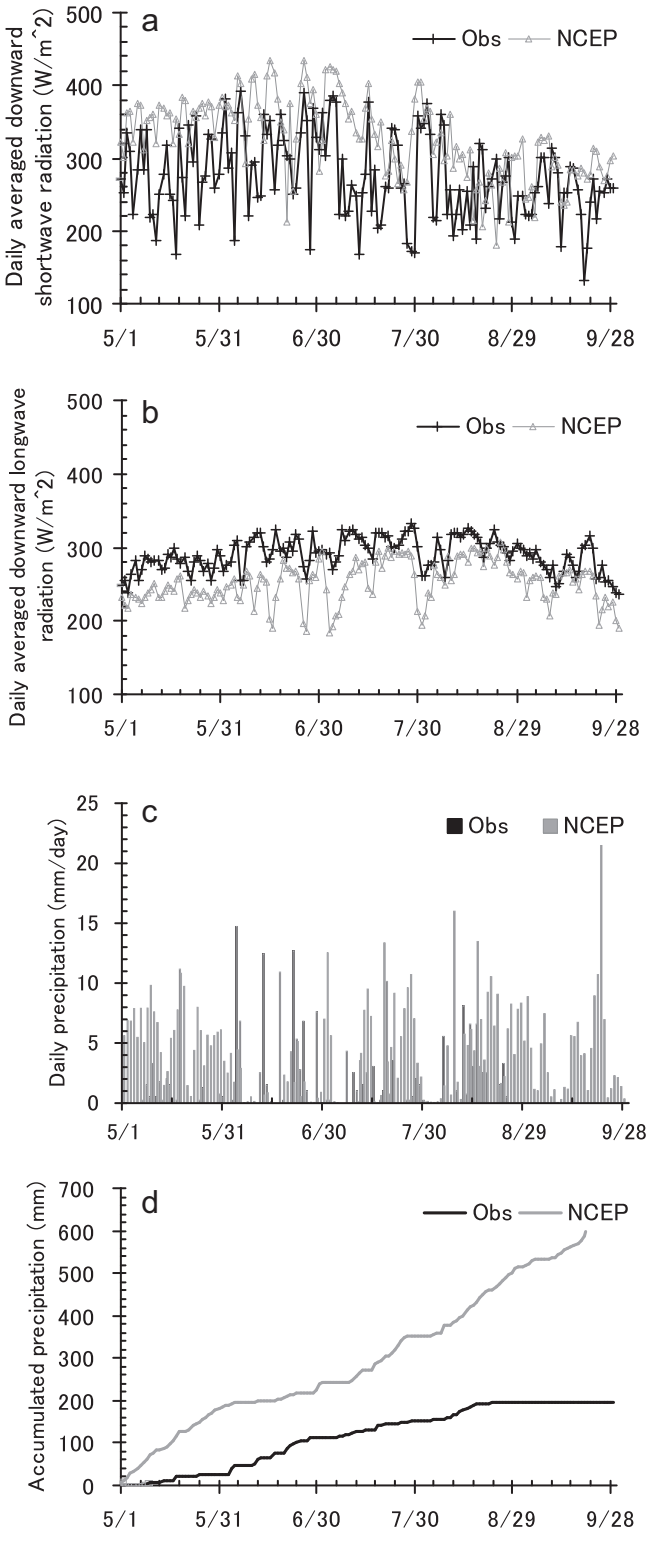

Fig. 1. Daily averaged meteorological forcing variables at Gaize: the downward shortwave radiation (a), downward longwave radiation (b), rain rate (c), and accumulated rainfall (d).

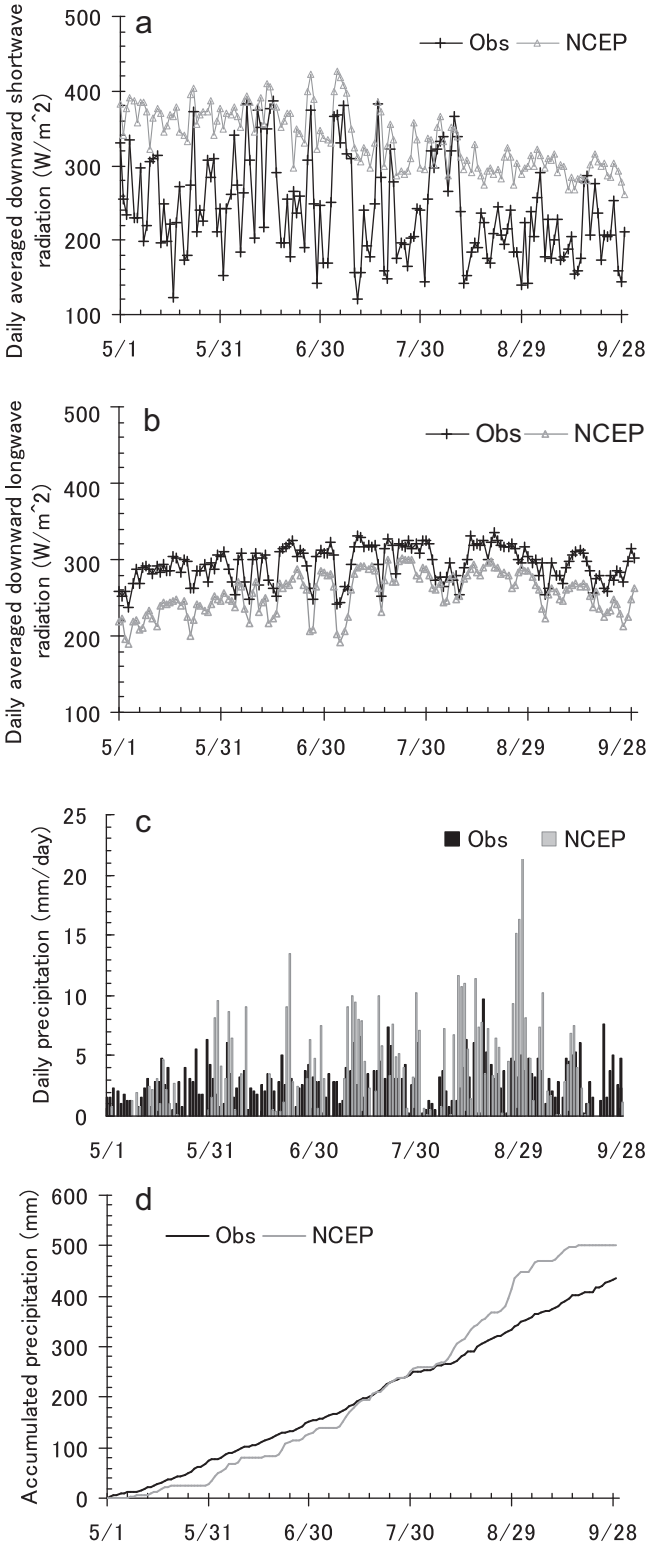

Fig. 2. Same as in Fig. 1, but for the Naqu station.

sensing provides the opportunity to measure the surface soil moisture at the regional, continental and even global scales. Passive microwave remote sensing provides a means for the direct measurement of the surface soil moisture (Njoku and Entekhabi, 1996) at a coarse resolution (which is on the order of approximately 50 km) and with a frequent temporal coverage (daily or bi-daily), which can partially satisfy the temporal resolution that is required for meteorological modeling. However, in the field of weather forecast and hydrology modeling, a finer temporal resolution would obviously improve the accuracy and reliability of the forecast.

Contrary to the limitations of *in situ* measurements and satellite remote sensing, numerical models can provide continuous estimates of soil moisture over the entire soil profile at any scale.

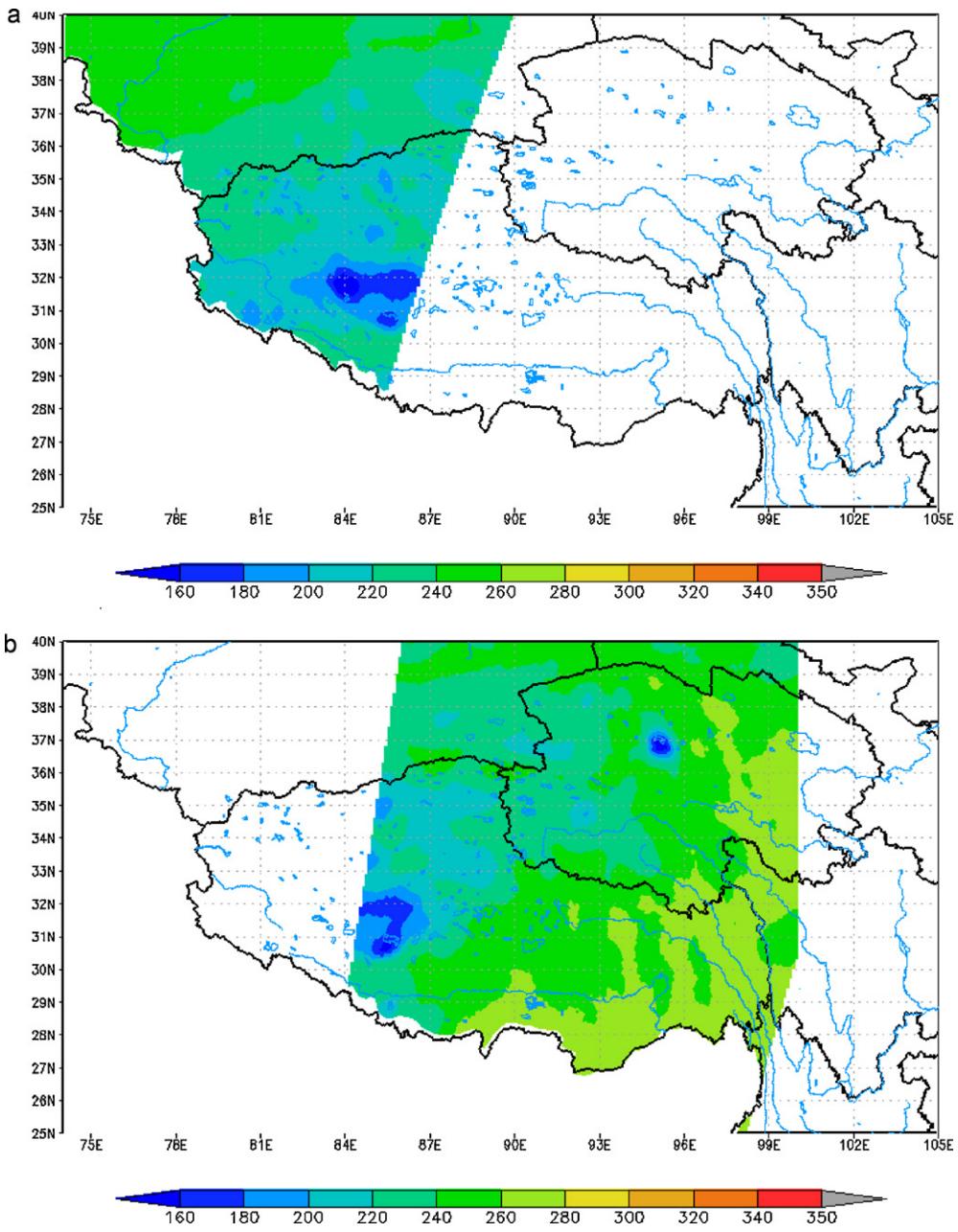

Fig. 3. Snapshot observation that was provided by the AMSR-E at the 6.925 GHz horizontal polarization channel on June 21st (a) and June 22nd (b), 2008.

However, due to the model initialization, the parameter and forcing errors, and the inadequate model physics and/or resolution, the model predictions are usually of low quality.

The LDAS, which merges the observation information (which includes *in situ* measurements and satellite remote sensing data) into a dynamic model (i.e., LSM), is expected to provide high-quality surface energy and water flux estimates with adequate spatial coverage and resolution for weather forecast (Reichle and Koster, 2005; Reichle et al., 2007). Compared with the atmospheric and oceanic data assimilation, the development of the LDAS was short and rapid. The development of the LDAS was initiated by using a simple direct insertion approach (Jackson et al., 1981) approximately 30 years ago. Currently, the LDAS uses a variety of sophisticated assimilation strategies, which include the variational assimilation strategy (Houser et al., 1998; Pathmathevan et al., 2003; Li et al., 2004; Dunne and Entekhabi, 2006) and the sequential assimilation strategy (Entekhabi et al., 1994; Walker and Houser, 2001; Reichle et al., 2002; Han and Li, 2008). From the view point of application scales, the LDAS initially started as field experiments for case studies (Houser et al., 1998; Reichle et al., 2001), but it has now extended to the regional scale, such as the European Land Data Assimilation System (ELDAS) (Van Den Hurk, 2002). Because the LDAS can make maximum usage of the observation data that are derived from satellite remote sensing, it is expected to improve the land surface water and energy simulations, especially in the ungauged and poorly gauged regions.

The Tibetan Plateau plays an important role in the progression of the Asian summer monsoon through its strong land-atmosphere interactions; it also influences circulations over China, the Northern Hemisphere and even the entire globe (Ma et al., 2009; Xu et al., 2008a; Yanai and Song, 1992; Yanai and Wu, 2006; Ye, 1981; Ye and Gao, 1979; Ye and Wu, 1998). Understanding the land-atmosphere interaction over the plateau is essential for weather forecast and climate change studies. Because it occupies a large area

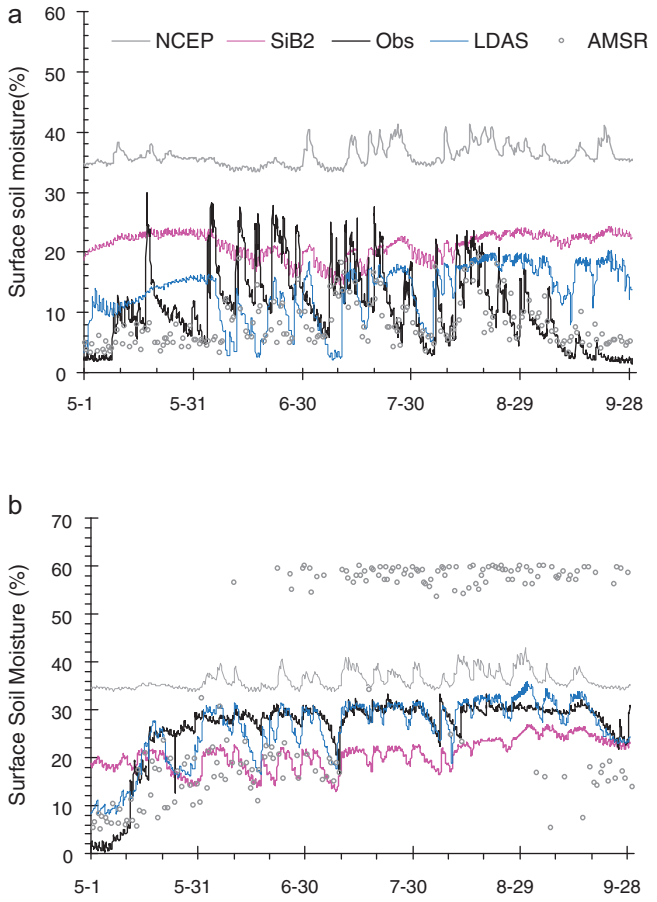

Fig. 4. Time series of the surface soil moisture at Gaize (a) and Naqu (b). Obs represents the *in situ* soil moisture observation; AMSR denotes the AMSR-E level 3 soil moisture product from JAXA; NCEP represents the soil moisture that was provided by the NCEP/NCAR reanalysis; LDAS represents the results from assimilation.

(approximately 1.2 million km^2) and has a high altitude (mean altitude of more than 4000 m above sea leave (asl)), the observation sites on the plateau are limited. Although many pioneering studies have been conducted there for decades, it is still a challenging task to represent the land surface energy and the water fluxes over the entire Tibetan Plateau.

The objective of this study was to develop an LDAS over the Tibetan Plateau by merging passive microwave remote sensing data and GCM output into a land surface model and to investigate the potential of the LDAS to improve the simulations of the land surface soil moisture and the energy flux. Specifically, the AMSR-E brightness temperature data and the NCEP reanalysis data were assimilated into the SiB2. In order to evaluate the capability of the assimilation system, the LDAS products, the SiB2 simulations, the NCEP simulations, and the AMSR-E retrievals were compared against the *in situ* observations. Performances of these four data sets were then intercompared. The logic behind this inter-comparison was as follows: (1) the contribution of the remote sensing data in the LDAS can be identified through the comparison between the LDAS and SiB2; (2) the role of the LSM in the LDAS can be identified through the comparison between the LDAS and AMSR-E; and (3) the capability of the LDAS to improve the land surface state estimation can be identified through the comparison between the LDAS and NCEP.

2. Data set

2.1. In situ stations and observations

The data that were observed at the Gaize and Naqu stations were used in this study; these data were obtained from the Japan International Cooperation Agency (JICA) China-Japan climate disasters mitigation project (JICA project) (Xu et al., 2008b). Gaize station (32°18′N, 84°06′E, 4416 m asl) is located in the middle of western Plateau, where the dry climate is dominant. The land cover at Gaize is bare soil with some sparse short grass. Naqu station (32°22′N, 91°54′ E, 4509 m asl) is located in the central Plateau, and it experiences a wet climate condition during the monsoon season. The Naqu site has a flat plateau grassy marsh land surface.

In this study, the land surface soil moisture and energy flux that were obtained at these two stations were used as the validation data. The spatial scales of the AMSR-E data (with a resolution around 50 km), the NCEP reanalysis data (with a resolution of roughly 210 km), the LSM, LDAS and the *in situ* observations were different from each other. Therefore, the direct comparison between these four data sets and the single *in situ* station data might be questionable. According to the design of the JICA project, these two stations were intentionally set up in mesoscale regions, which are relatively flat and are believed to be representative of the west and central Plateau, respectively. This design partly alleviates the representativeness problems that arise from the LDAS validation.

Two sets of automatic weather stations (AWSs) have been installed in Gaize and Naqu. The soil moisture that was measured with an horizontally installed TDR probe at a 5-cm depth from the surface was used for the surface soil moisture validation. The other meteorological variables were used to calculate the surface energy components, i.e., the sensible heat (Hs) flux and the latent heat (LE) flux by the Bowen Ratio Energy Balance (BREB) method (Fritschen and Simpson, 1989), as:

$$\mathrm{LE} = \frac{R_\mathrm{n} - G}{1 + B} \tag{1}$$

$$\mathrm{Hs} = \frac{B * (R_\mathrm{n} - G)}{1 + B}, \tag{2}$$

where R_n is net radiation, G is ground heat flux and B is Bowen Ratio

$$B \cong \frac{(C_\mathrm{p}/\lambda) * (T_1 - T_2)}{q_1 - q_2} \tag{3}$$

with C_p is specific heat capacity at a constant pressure, λ is latent heat of vaporization, T_1, T_2 and q_1, q_2 are the temperature and specific humidity at two levels, respectively. The derived latent heat flux and sensible heat flux, together with the *in situ* observed ground heat flux, were used as the *in situ* energy flux observations.

Table 1
Statistic metrics of the daily NCEP forcing data.

Items	Naqu			Gaize		
	MBE	RMSE	*R*	MBE	RMSE	*R*
DSW (W/m^2)	95.83	108.78	0.631	53.94	82.89	0.364
DLW (W/m^2)	−37.96	41.09	0.813	−38.24	44.37	0.630
Rain rate (mm/d)	0.43	3.90	0.319	2.83	5.55	−0.009
Accumulated rain (mm)	14.10	48.39	0.991	195.77	222.43	0.941

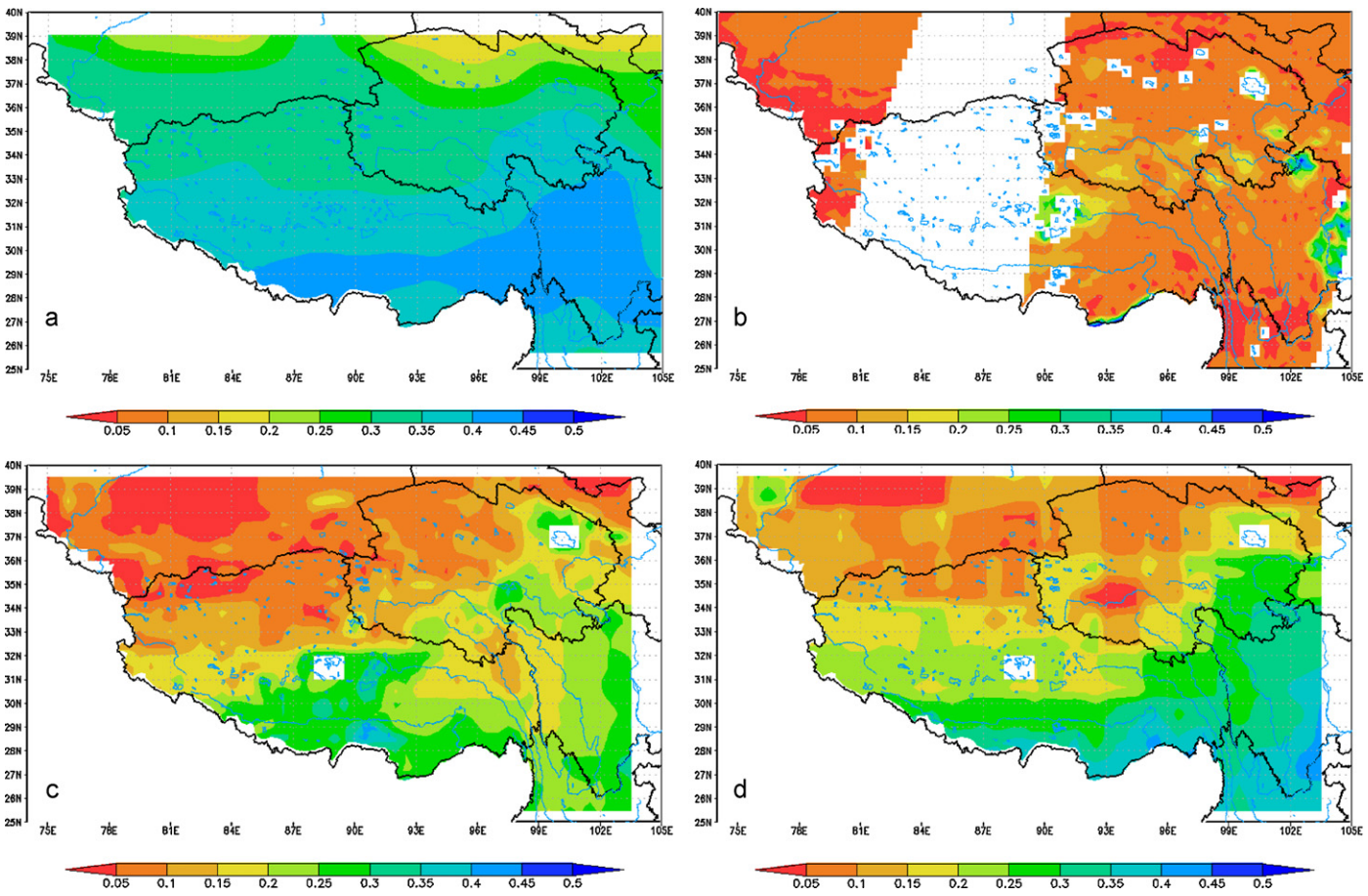

Fig. 5. Comparison of the daily averaged surface soil moisture that was simulated by the NCEP (a), AMSR-E (b), LDAS (c) and SiB2 (d) over the Tibetan Plateau on Jun 22nd, 2008.

2.2. Meteorological forcing data: NCEP reanalysis

The National Centers for Environmental Prediction/National Center for Atmospheric Research (NCEP/NCAR) reanalysis (which is referred to as the NCEP reanalysis hereafter) is a global reanalysis that was initiated in 1948 and continues to the near real-time at a horizontal resolution of T62 and a temporal resolution of 6 h (Kalnay et al., 1996). The dynamic model that is used in the NCEP reanalysis is the NCEP global spectral model (Kanamitsu, 1989; Kalnay et al., 1990; Kanamitsu et al., 1991), in which the land surface processes are treated as portions of the atmospheric model in a relatively simple approach. Based on the merits of the NCEP reanalysis data, such as the data availability, the ease of access and the good spatial and temporal coverage, we used these data as the meteorological forcing data in this study. The meteorological forcing data, which included the downward shortwave and longwave radiation, the air temperature at 2 m above the land surface, the wind speed, the surface pressure, the specific humidity and the rain rate, spatially and temporally interpolated to generate an hourly forcing data at 50 km resolution.

Figs. 1 and 2 show the comparisons between the daily averaged NCEP forcing data and the data that were observed at Gaize and Naqu, respectively. It was clear that the NCEP generally overestimated the downward shortwave radiation data, while it underestimated the downward longwave radiation data. The NCEP rain rate data from the Naqu station were acceptable, but the data from Gaize were seriously biased. This was in agreement with pervious studies (Berg et al., 2003). As indicated in Table 1, even for the daily averaged values, the correlation coefficient (R) of the rain rate was very small, and the mean bias error (MBE) of the accumulated rain was very large at the Gaize station, which implies that the rainfall input may introduce large errors into the LDAS simulation. The NCEP reanalysis also provides land surface states and fluxes, which include the soil moisture at 0–10 cm, the latent heat flux, the sensible heat flux and the ground heat flux. This data were subset to illustrate the general land surface status that is used in the current GCMs.

2.3. AMSR-E brightness temperature and soil moisture products

The brightness temperatures of the AMSR-E that were observed at 6.925 GHz and 18.7 GHz were used as the observation data in the LDAS, considering there is little radio frequency interference (RFI) effect at these frequencies in this region. The observation times of AMSR-E are local noon and midnight. In this application, only the midnight observation data were used as the land surface temperature profile was almost uniform at this overpass time. The assimilation window of the assimilation system was, therefore, decided as one day. The resolution of the system was also decided by the 0.5° resolution of the AMSR-E data.

Fig. 3 provides two examples of the AMSR-E midnight observation at the 6.925 GHz horizontal channel for two consecutive days. Over a large domain like the Tibetan Plateau, it is difficult for the AMSR-E to cover whole study area with one scan. Therefore, the satellite observation was not always available in all regions at the same time.

Land surface variables, which includes surface soil moisture, soil temperature and vegetation water content, can be directly

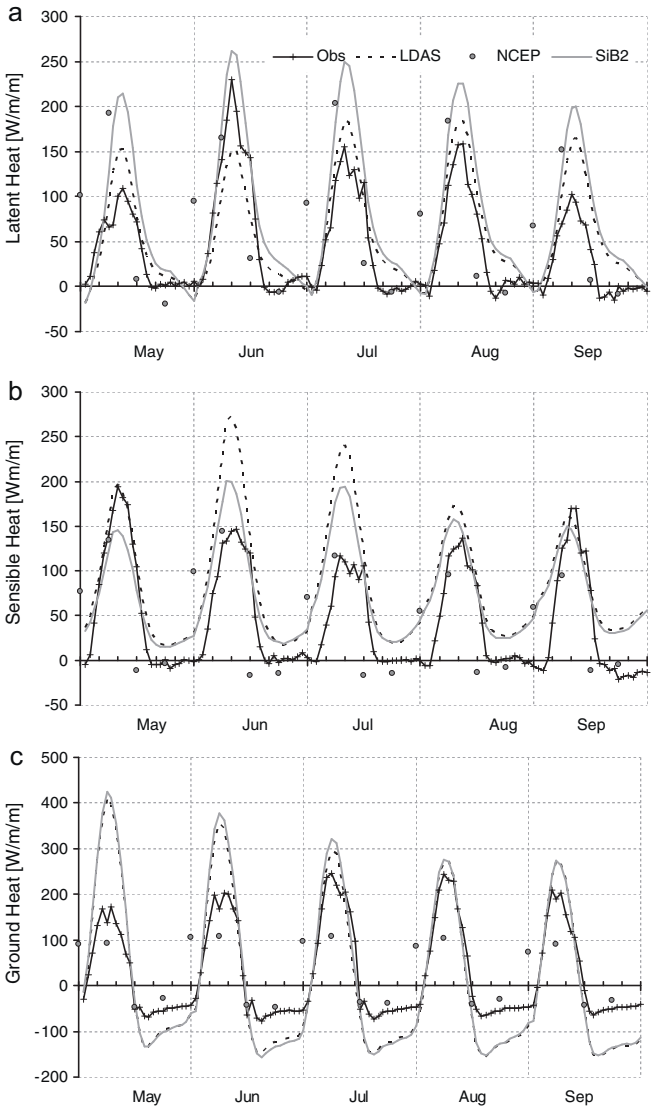

Fig. 6. Monthly averaged diurnal cycles of the latent heat flux (a), sensible heat flux (b), and ground heat flux (c) at the Gaize station.

estimated from AMSR-E brightness temperature data by using various algorithms (Njoku et al., 2003; Paloscia et al., 2006). The AMSR-E soil moisture retrievals that were produced by the Japan Aerospace Exploration Agency (JAXA) were used in this study (Lu et al., 2009; Fujii et al., 2009). This data set was used to represent the state-of-art estimation of the land surface status that was provided by microwave remote sensing. By comparing LDAS simulation with the AMSR-E soil moisture retrievals, the superiority of the LDAS product to the satellite data can be identified.

3. Land data assimilation system

3.1. Components of the LDAS

The LDAS that was used in this study is an updated version of Yang et al. (2007), and it consists of a LSM, which is used to forecast the land surface status and calculate surface fluxes, an observation operator (i.e., a radiative transfer model (RTM)), which can simulate the microwave brightness temperature for the corresponding land surface status, and an optimization scheme, which is used to search for optimal values of soil moisture while minimizing the difference between the simulated and observed brightness temperatures.

The LSM was the SiB2 (Sellers et al., 1986, 1996), which contained some modifications regarding the heat and momentum transfer simulation for the bare soil (Yang et al., 2002) and for the sparse canopy (Watanabe and Kondo, 1990). The SiB2 was selected as the dynamic model based on the following criteria: (1) its successful application on the Tibetan Plateau (Gao et al., 2004; Li et al., 2004; Hong and Kim, 2010); (2) its experiences in global scale application (Sato et al., 1989); and (3) its relatively simple two-layer structure that allowed for an easy application in the data assimilation system. The soil column of SiB2 was discretized into the three following layers: the surface layer (0–5 cm depth), the root zone layer (5–20 cm depth) and the deep soil layer (20–200 cm depth). The complete formulation of the SiB2 was described by Sellers et al. (1986, 1996).

The observation operator that was used in this study is an extended RTM that includes the following: (1) a soil media radiative model (Lu et al., 2009), which counts the volume scattering effects of the dry soil particles and the influence of the moisture and temperature profile; (2) an advanced integral equation method (AIEM) (Chen et al., 2003), which accounts for the surface

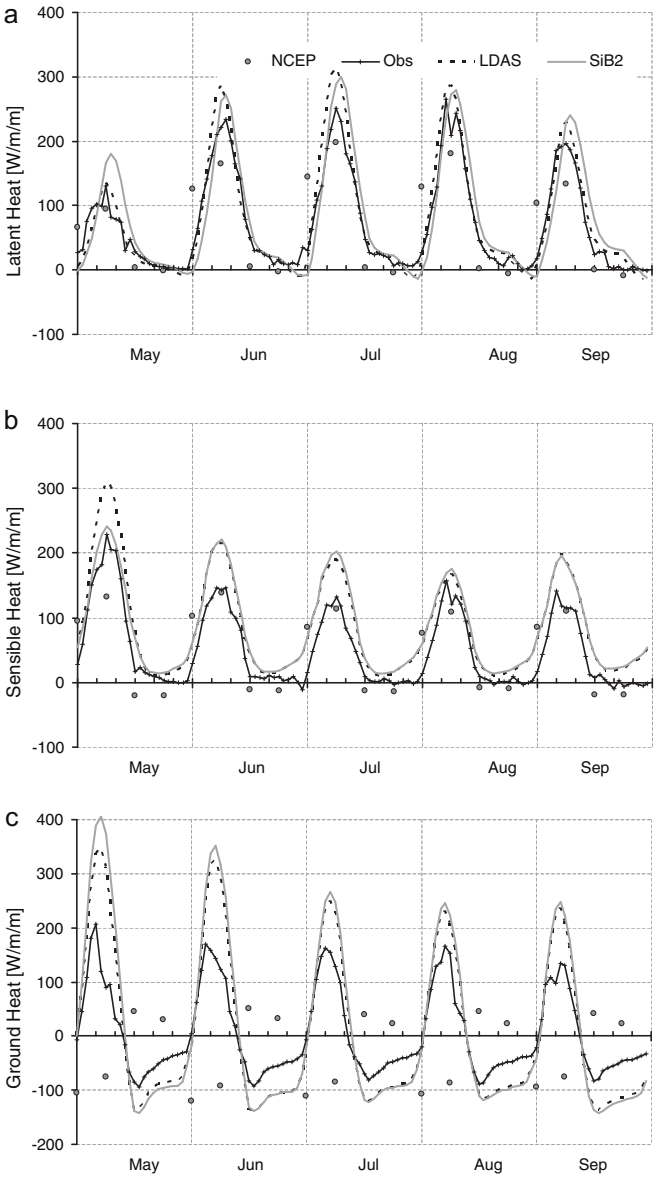

Fig. 7. Same as in Fig. 8, but at the Naqu station.

roughness effects; and (3) the Tau-Omega model (Jackson and Schmugge, 1991), which accounts for the vegetation effects. The downward radiation from the vegetation and the atmosphere, which are reflected by the soil surface, was neglected because the reflection at the soil surface was much smaller than the emission from the surface. Furthermore, because the atmosphere is almost transparent to the low frequencies of the microwave region (Ulaby et al., 1986), the atmospheric effect was also neglected. The optimization scheme that was used is the shuffled complex evolution (SCE) method (Duan et al., 1993).

3.2. Algorithm of LDAS

The LDAS used here adopts a two-pass technique to implement both parameter optimization and the land data assimilation. In pass 1, which runs continuously for a period of approximately two months, the soil parameters that were used in the LSM and RTM were optimized. The cost function of the parameter optimization is shown in eq. (4) as the following:

$$\mathrm{COST} = \sum_{i=1}^{n}\sum_{j=1}^{2}[\mathrm{TB}_{\mathrm{obs},i}(f_j,p) - \mathrm{TB}_{\mathrm{sim},i}(f_j,p)]^2 \quad (4)$$

where n is the number of AMSR-E observations during the optimization window (approximately 2 months); $\mathrm{TB}_{\mathrm{obs}}$ represents the observed brightness temperature by the AMSR-E; $\mathrm{TB}_{\mathrm{sim}}$ represents the simulated brightness temperature by the RTM; f is the frequency, $f_1 = 6.925$ GHz, $f_2 = 18.7$ GHz; and p is the polarization. By minimizing the costs, the parameter sets including the soil porosity, the soil texture (percentage of sand and clay), the surface roughness parameters, and the vegetation RTM parameters, were optimized.

After obtaining the soil parameters through pass 1, the normal land data assimilation was implemented through a variational way, which directly assimilated radiance (brightness temperature) into the LSM (SiB2) using the observation operator (RTM). The surface soil moisture status in the LSM was updated at the initial time of each assimilation cycle (approximately 1 day) by minimizing the cost function of the assimilation pass as follows:

$$\mathrm{COST} = \sum_{j=1}^{2}\{[\mathrm{TB}_{\mathrm{obs}}(f_j,p) - \mathrm{TB}_{\mathrm{sim}}(f_j,p)]^2 + [\mathrm{TB}_0(f_j,p) - \mathrm{TB}_{0,\mathrm{bg}}(f_j,p)]^2\} \quad (5)$$

where TB_0 and $TB_{0,bg}$ are the simulated brightness temperatures using the renewed soil moisture and the background soil moisture, respectively. In the assimilation pass, only the surface soil moisture was optimized. It was decided by considering the following facts: (1) the AMSR-E could only receive the electromagnetic signals emitted from the top few centimeters of soil (roughly less than 5 cm); (2) the AMSR-E brightness temperature is more sensitive to the soil moisture than the soil physical temperature; and (3) there are only four observations available in the one-day assimilation window and it is thus difficult to optimize any other variable than the surface soil moisture.

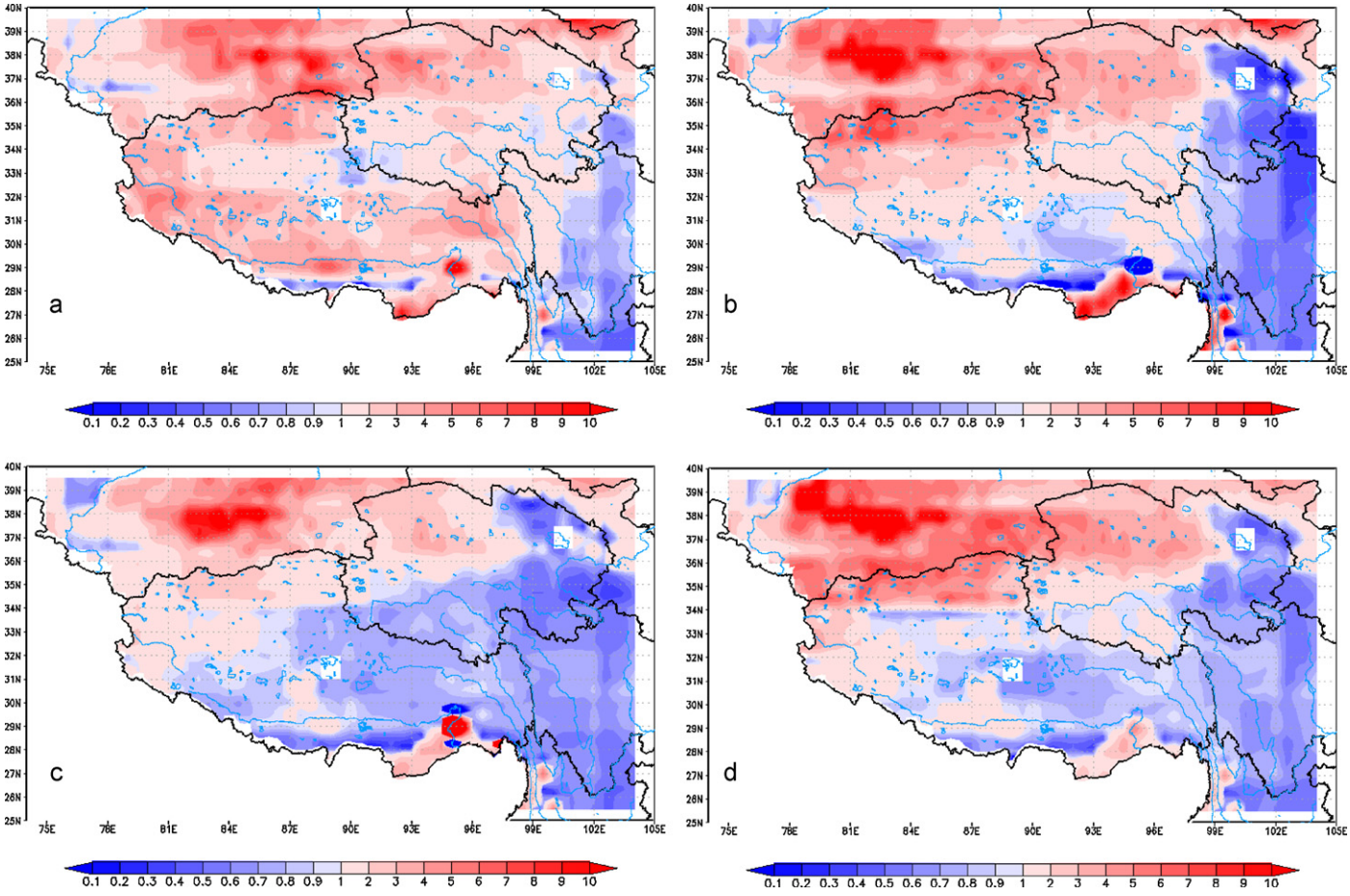

Fig. 8. Comparison of the ten-day average Bowen ratio over the Tibetan Plateau for the LDAS ((a) for the period from May 21 to 31, (b) for the period from June 21 to 30, (c) for the period from July 21 to 31, (d) for the period from August 21 to 31, and (e) for September 21 to 30) and the NCEP ((f) for the period from May 21 to 31, (g) for the period from June 21 to 30, (h) for the period from July 21 to 31, (i) for the period from August 21 to 31, and (j) for September 21 to 30)).

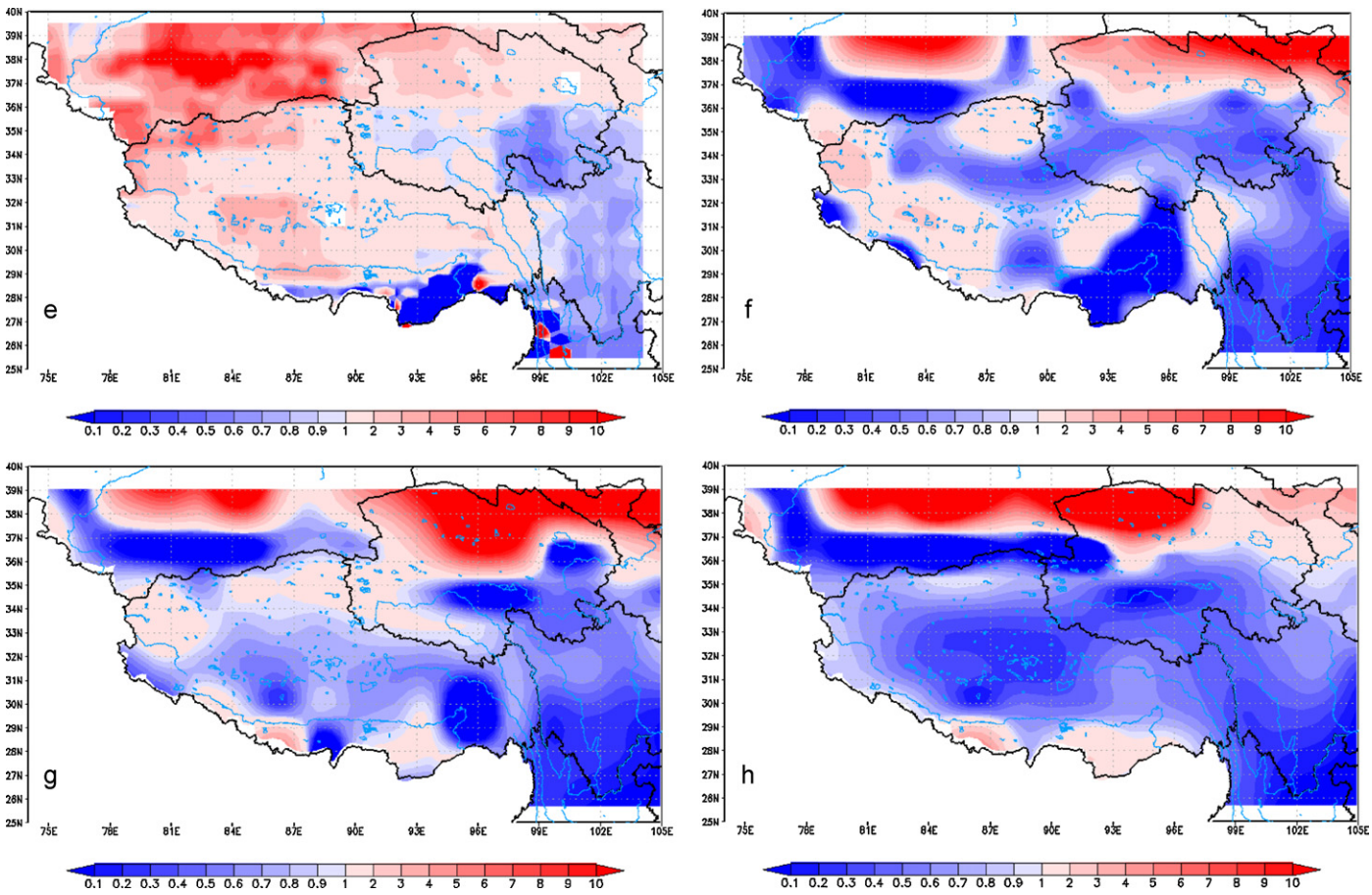

Fig. 8. (*continued*)

3.3. Parameters of the LDAS

In this study, global parameter databases were used to obtain the default parameters; for instance, the default soil parameters and the land cover characteristics were derived from the International Satellite Land-Surface Climatology Project (ISLSCP) initiative II (Hall et al., 2005). Due to the lack of *in situ* observations, the default morphological parameters of the Agriculture/C3 grassland and the aerodynamic parameters that were required to run SiB2 were derived from Sellers et al. (1996) and were fixed during the entire simulation period.

The time-space varying vegetation information, which is required in the SiB2 and RTM, were derived from the MODIS (Moderate Resolution Imaging Spectroradiometer) 8-day Leaf Area Index (LAI) products, which were converted to 0.5×0.5 degrees resolution and interpolated to daily values.

4. Results and discussion

The LDAS was run over the entire Tibetan Plateau, using NCEP as the atmospheric forcing data and the AMSR-E brightness temperatures as the observations. The simulation period was from May 1st to September 30th, 2008, which covering the whole monsoon season. To check the influences of the remote sensing data in the LDAS, the LSM (SiB2) using the NCEP reanalysis data alone was compared. The output of this LSM run was named SiB2. Soil moisture from the four data sets, NCEP, AMSR-E, SiB2 and LDAS, were first compared against the *in situ* observations at two local stations. Inter-comparison of the regional soil moisture distributions among the four data sets was then conducted. For the surface energy fluxes, similar analyses were performed.

4.1. Validation of the soil moisture with the in situ observations

Fig. 4a and b show the local scale comparison results from Gaize station and Naqu station, respectively. Table 2 summarizes the RMSE, MBE, and R of the four data sets. Compared to the *in situ* station data, the NCEP reanalysis data generally overestimated the soil moisture mean values, while they underestimated its variation ranges at both of the sites. The bias was larger at Gaize than at Naqu, which corresponds to the larger rainfall errors that were observed at Gaize and are shown in Fig. 1 and Table 1. For both of the stations, the RMSE and MBE of the NCEP were larger than 10% (vol/vol). This result suggests that the land surface status that was presented by the NCEP was not reliable at both of the locations.

The AMSR-E retrievals were in good agreement with the *in situ* observations that were performed at Gaize station; they contained the smallest MBE and RMSE and the largest *R*. However, the

Table 2
Statistic metrics of the estimated surface soil moisture (vol/vol, in %).

Data sources	Gaize			Naqu		
	MBE	RMSE	*R*	MBE	RMSE	*R*
LDAS	2.74	8.46	0.361	−0.17	3.88	0.853
AMSR-E	−3.01	6.13	0.601	10.16	21.25	0.562
NCEP	25.28	26.13	0.442	10.02	12.15	0.417
SiB2	10.35	12.59	−0.243	−5.52	8.94	0.315

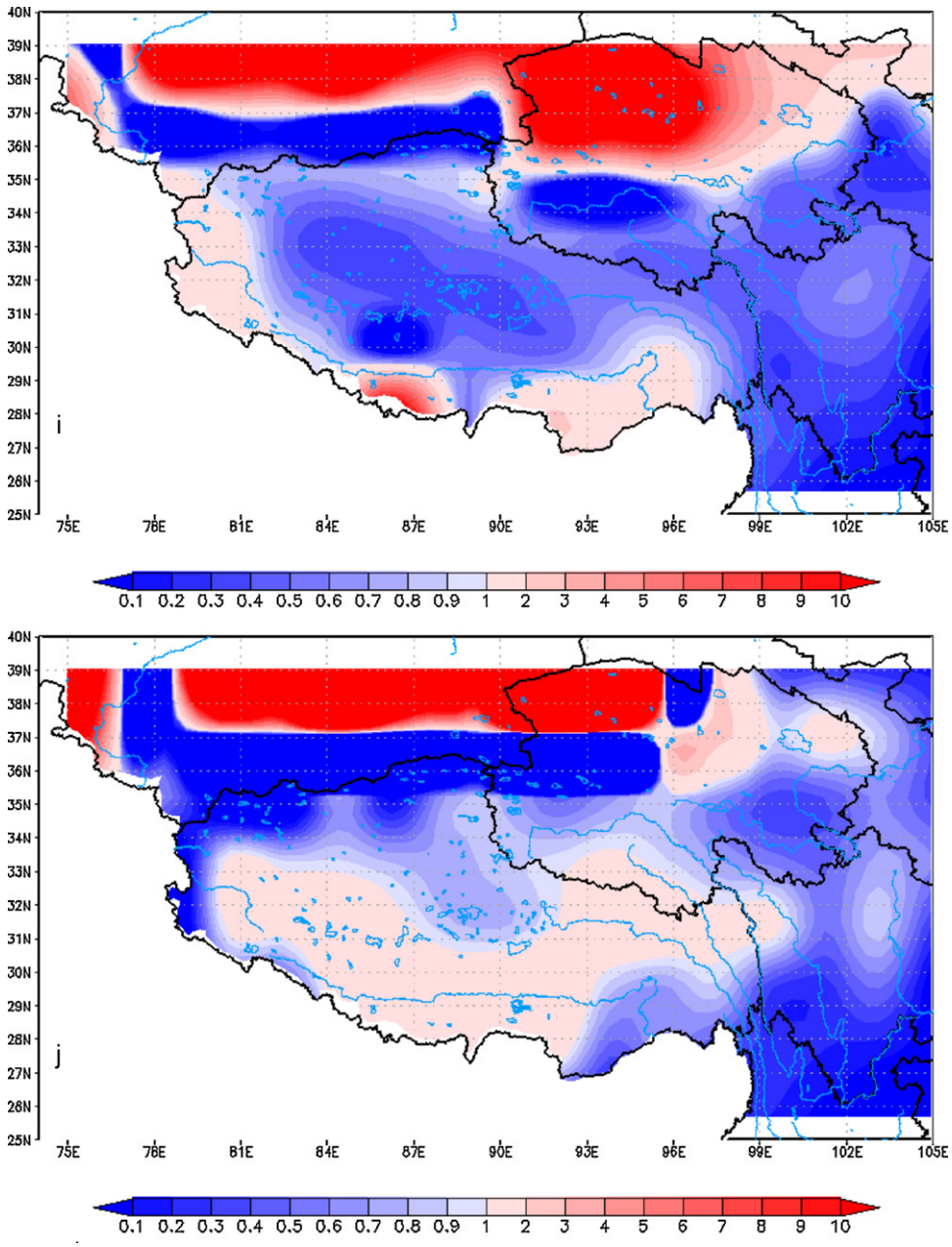

Fig. 8. (*continued*)

AMSR-E did not fit the soil moisture variation trends that were observed at Naqu station; these results contained the largest MBE and RMSE. This unstable performance was not an uncommon case for satellite retrievals, and hinders the application of the AMSR-E soil moisture products worldwide. This is one reason why brightness temperature were assimilated directly in this study, rather than the soil moisture retrievals.

The SiB2 performed better than the NCEP, but it overestimated the soil moisture at Gaize station and underestimated at the soil moisture at Naqu station. Further, the SiB2 showed the weakest correlation to the *in situ* data at both stations. This result implies that reliable land surface estimations cannot be obtained by just simply running an LSM with atmosphere forcing from a GCM output.

Compared to the NCEP and the SiB2 data, the soil moisture simulation of the LDAS was much improved. The LDAS provided the best estimates at Naqu, which showed a significantly decreased MBE and RMSE and a significantly increased R. However, for Gaize, although the surface soil moisture was improved in quantity (the RMSE decreased by two-thirds), it showed a poor correlation with the observations. We believe this result was caused by the strong forcing errors that were inherited from the biased rainfall input, and we suggest that reasonable forcing data are needed to properly estimate the temporal variations.

4.2. Inter-comparison of the regional soil moisture estimates over the Tibetan Plateau

Fig. 5 shows the daily soil moisture over the Tibetan Plateau on June 22nd 2008, from the NCEP, AMSR-E, LDAS and SiB2, respectively. It is clear that the NCEP produced a wetter and more homogenous soil moisture distribution than the AMSR-E, LDAS and SiB2. Although the AMSR-E retrieval showed more spatial variation, it failed to provide full coverage, which can partly be attributed to the limitation of the sensor, the platform and the algorithm. In

Table 3
Statistic metrics of the monthly averaged diurnal surface energy fluxes (in W/m^2) that were simulated by the LDAS.

	Gaize			Naqu		
	MBE	RMSE	*R*	MBE	RMSE	*R*
Hs	43.38	54.21	0.88	35.64	42.36	0.93
LE	12.88	31.05	0.88	6.93	35.14	0.98
G0	−15.09	77.19	0.95	3.72	68.85	0.97

contrast, the SiB2 was able to provide a soil moisture estimation for the whole plateau. By integrating the advantages of the LSM and the remote sensing data, the LDAS provided a comprehensive and more realistic soil moisture distribution. For example, the LDAS estimated that the soil moisture was less than 5% (vol/vol) in two desert regions, the Taklamakan desert (37°–40°N, 78°–85°E) and the Chaidamu desert (35°–40°N, 92°–96°E); however, in the two desert, the NCEP simulations generally predicted a soil moisture that was larger than 20% (vol/vol), and the SiB2 simulations predicted a moisture that was approximately 10% (vol/vol). Moreover, AMSR-E can only provide two observations per day, while the LDAS can generate hourly soil moisture. Compared to the AMSR-E soil moisture products, the LDAS can therefore provide more information regarding the spatial and temporal variation of the surface soil moisture.

4.3. Intercomparison of the surface energy fluxes as simulated by the LDAS and the NCEP

Figs. 6 and 7 show the monthly averaged diurnal variation of the latent heat flux, the sensible heat flux, and the ground heat flux at Gaize and Naqu, respectively. The NCEP simulations are also plotted, but one should keep in mind that the value provided by the NCEP is 6 h average. From Figs. 6 and 7, the following results were derived: (1) among the three surface energy components, the latent heat flux was best estimated by the LDAS; (2) the LDAS generally overestimated the sensible heat flux at both of the stations; (3) the LDAS produced a bigger range for the ground heat flux; and (4) the LDAS performance was better at the Naqu station than at Gaize.

As listed in Table 3, the RMSE of the latent heat flux estimates was the smallest, the sensible heat flux was intermediate, and the ground heat flux was the largest. This result suggests that the skill of the latent heat flux estimates from the LDAS was better than the sensible heat flux, which was superior to the ground heat flux. This performance may be partly attributed to the design of the LDAS: only the surface soil moisture status were corrected directly, this impacting the latent heat flux calculation more obviously than the sensible heat flux calculation.

As shown in Tables 3 and 4, compared to the SiB2 simulation, the LDAS generally improved the latent heat flux and the ground heat flux estimations. For the latent heat flux simulation, the LDAS decreased the RMSE from the SiB2 at Gaize by more than one-third (17 W/m^2). For the ground heat flux, the LDAS decreased RMSE by about one-sixth (14 W/m^2). Both the LDAS and the SiB2 overestimated the sensible heat flux, which is partly due to that LSM does not accounting for the excess resistance that is important for the sensible heat flux calculation (Yang et al., 2009), and should be addressed in future research.

Table 4
Statistic metrics of the monthly averaged diurnal surface energy fluxes (in W/m^2) that were simulated by the SiB2.

	Gaize			Naqu		
	MBE	RMSE	*R*	MBE	RMSE	*R*
Hs	29.93	42.17	0.87	34.39	39.72	0.96
LE	34.32	48.36	0.93	9.73	36.17	0.93
G0	−10.39	81.18	0.95	9.05	82.22	0.96

4.4. Regional Bowen ratio distribution

Fig. 8 shows the ten-day averaged Bowen ratio distribution over the plateau, and this was calculated for the last 10 days of each month from May to September. As shown in Fig. 8a–e, there was an obvious temporal variation in the Bowen ratio that was simulated by the LDAS. The variation was closely related to the monsoon activities over the Tibetan Plateau. Fig. 8a depicts the high Bowen ratio values; this result indicates that the sensible heat flux was dominant in May, and that the land surface was dry during the pre-monsoon season. As the monsoon began and progressed during June and July (Fig. 8b and c), the Bowen ratio decreased and the latent heat flux became gradually dominant. During the post-monsoon season (Fig. 8d and e), as the monsoon fading, the Bowen ratio increased, and the sensible heat flux was once again dominant. However, the Bowen ratio (Fig. 8f–j) that was generated from the NCEP reanalysis did not show this clear variation.

A clear contrast in the Bowen ratio distribution over the plateau can be observed in the LDAS simulation (Fig. 8b–d); the Bowen ratio was low in the southeast and high in the northwest. This is in response to that the Plateau was wet in the southeast regions while it was dry in the northwest regions. These findings are also supported by the daily soil moisture field (Fig. 5c) and the ten-day average soil moisture field that was provided by the LDAS (data not shown). These contrasting land surface statuses and energy flux distribution characteristics could be explained by the well-known atmospheric activities: during the Asian monsoon, cyclones bring moisture from the Bay of Bengal to the southeast of the plateau, and they bring dry air masses from the Taklamakan desert to the northwest of the plateau.

5. Conclusion

This study showed that it is possible to improve the land surface energy and water flux estimates by merging the AMSR-E observations and the NCEP reanalyses in a LDAS. The results of this simulation were validated at two stations by comparing these data against the *in situ* soil moisture and energy flux observations. The LDAS generally simulated the surface soil moisture well; the MBE was less than 3% (vol/vol), and the RMSE was less than 8% (vol/vol). Compared to the performance of the NCEP and SiB2, the LDAS was clearly able to partially reduce the errors that were inherited from the biased forcing data. For the surface energy components, the accuracy of the latent heat flux and the ground heat flux simulations were improved; the RMSE decreased by 1/3 and 1/6, respectively.

For simulations over the whole Tibetan Plateau, the regional distribution of the surface soil moisture and the Bowen ratio that was generated by the LDAS corresponds well to the climatic pattern on the Tibetan Plateau, which provides a more realistic monsoon cycle than that were generated by the NCEP. Moreover, the comparison between the LDAS soil moisture and the AMSR-E products demonstrated that the LDAS was able to provide more comprehensive data in the regions and/or during the periods that the satellite fails to provide observations. Therefore, the land surface water and Bowen ratio data sets that were generated by the LDAS are superior to those that were provided by the NCEP, SiB2 and AMSR-E. This data set would provide an opportunity to study the land atmosphere interactions and the potential to improve the understanding of the climate and weather system over the Tibetan Plateau.

In this study, all the data and parameters were obtained from the global data set as follows: the meteorological forcing data were obtained from the NCEP; the satellite remote sensing data were

obtained from the AMSR-E; the vegetation data were obtained from the MODIS; and the default parameters were obtained from the ISLSCP II. All of these data are globally available, publicly accessible and free. Therefore, the LDAS could be easily applied to any region, and the experiences earned from this study are also useful for ungauged or poorly gauged regions.

Acknowledgements

This study was performed as a part of the China and Japan intergovernmental cooperation program (JICA project). We would like to thank our local colleagues from the China Meteorology Administration and the China Academy of Science at the Naqu and Gaize stations.

References

Berg, A.A., Famiglietti, J.S., Walker, J.P., Houser, P.R., 2003. Impact of bias correction to reanalysis products on simulations of North American soil moisture and hydrological fluxes. Journal of Geophysical Research 108 (D16), 4490–4505, doi:10.1029/2002JD003334.

Betts, A.K., Ball, J.H., Beljaars, A.C.M., 1996. The land surface-atmosphere interaction: a review based on observational and global modeling perspectives. Journal of Geophysical Research 101, 7209–7225.

Chen, K.S., Wu, T.D., Tsang, L., Li, Q., Shi, J.C., Fung, A.K., 2003. Emission of rough surfaces calculated by the integral equation method with comparison to three-dimensional moment method simulations. IEEE Transactions on Geoscience and Remote Sensing 41, 90–101.

Delworth, T., Manabe, S., 1988. The influence of potential evaporation on the variabilities of simulated soil wetness and climate'. Journal of Climate 1, 523–547.

Duan, Q., Gupta, V.K., Sorooshian, S., 1993. A shuffled complex evolution approach for effective and efficient global minimization. Journal of Optimization Theory and Application 76, 501–521.

Dunne, S., Entekhabi, D., 2006. Land surface state and flux estimation using ensemble Kalman smoother during the Southern Great Plains 1997 field experiment. Water Resources Research 42, W01407, doi:10.1029/2005WR004334.

Entekhabi, D., Nakamura, H., Njoku, E.G., 1994. Solving the inverse-problem for soil moisture and temperature profiles by sequential assimilation of multifrequency remotely sensed observations. IEEE Transactions on Geoscience and Remote Sensing 32 (2), 438–448.

Entekhabi, D., Rodrigues-Iturbe, I., Castelli, F., 1996. Mutual interaction of soil moisture state and atmospheric processes. Journal of Hydrology 184, 3–17.

Fritschen, L.J., Simpson, J.R., 1989. Surface-energy and radiation balance systems—general description and improvements. Journal of Applied Meteorology 28 (7), 680–689.

Fujii, H., Koike, T., Imaoka, K., 2009. Improvement of the AMSR-E algorithm for soil moisture estimation by introducing a fractional vegetation coverage dataset derived from MODIS data. Journal of The Remote Sensing Society of Japan 29, 282–292.

Gao, Z., Chae, N., Kim, N., Hong, J., Choi, J., Lee, T.H., 2004. Modeling of surface energy partitioning, surface temperature, and soil wetness in the Tibetan prairie using the Simple Biosphere Model 2 (SiB2). Journal of Geophysical Research 109, D06102, doi:10.1029/2003JD004089.

Hall, F.G., Collatz, G.J., Los, S.O., Brown, E., Colstoun, D.E., Landis, D., 2005. ISLSCP Initiative II: DVD/CDROM: NASA.

Han, X., Li, X., 2008. An evaluation of the nonlinear/non-Gaussian filters for the sequential data assimilation. Remote Sensing of Environment 112 (4), 1434–1449, doi:10.1016/j.rse.2007.07.008, ISSN 0034-4257.

Hong, J., Kim, J., 2010. Numerical study of surface energy partitioning on the Tibetan plateau: comparative analysis of two biosphere models. Biogeosciences 7, 557–568, doi:10.5194/bg-7-557-2010.

Houser, P.R., Shuttleworth, W.J., Famiglietti, J.S., Gupta, H.V., Syed, K.H., Goodrich, D.C., 1998. Integration of soil moisture remote sensing and hydrologic modeling using data assimilation. Water Resources Research 34, 3405–3420.

Jackson, T.J., Schmugge, T.J., Nicke, A.D., Coleman, G.A., Engman, E.T., 1981. Soil moisture updating and microwave remote sensing for hydrological simulation. Hydrological Sciences Bulletin 26 (3), 305–319.

Jackson, T.J., Schmugge, T.J., 1991. Vegetation effects on the microwave emission of soils. Remote Sensing of Environment 26, 203–212.

Kalnay, E., Kanamitsu, M., Kistler, R., Collins, W., Deaven, D., Gandin, L., Iredell, M., Saha, S., White, G., Woollen, J., Zhu, Y., Chelliah, M., Ebisuzaki, W., Higgins, W., Janowiak, J., Mo, K.C., Ropelewski, C., Wang, J., Leetmaa, A., Reynolds, R., Jenne, R., Joseph, D., 1996. The NCEP/NCAR 40-year reanalysis project. Bulletin of the American Meteorological Society 77, 437–471.

Kalnay, E., Kanamitsu, M., Baker, W.E., 1990. Global numerical weather prediction at the National Meteorological Center. Bulletin of the American Meteorological Society 71, 1410–1428.

Kanamitsu, M., 1989. Description of the NMC global data assimilation and forecast system. Weather and Forecasting 4, 335–342.

Kanamitsu, M., Alpert, J.C., Campana, K.A., Caplan, P.M., Deaven, D.G., Iredell, M., Katz, B., Pan, H.-L., Sela, J., White, G.H., 1991. Recent changes implemented into the global forecast system at NMC. Weather and Forecasting 6, 425–435.

Koster, R., Suarez, M., Higgins, R., van den Dool, H., 2003. Observational evidence that soil moisture variations affect precipitation. Geophysical Research Letters 30 (5), 1241, doi:10.1029/2002GL016571.

Koster, R.D., 2004. GLACE team members, Regions of strong coupling between soil moisture and precipitation. Science 305, 1138–1140.

Li, X., Koike, T., Pathmathevan, M., 2004. A very fast simulated re-annealing (VFSA) approach for land data assimilation. Computers and Geosciences 30 (3), 239–248.

Lu, H., Koike, T., Fujii, H., Ohta, T., Tamagawa, T., 2009. Development of a physically-based soil moisture retrieval algorithm for spaceborne passive microwave radiometers and its application to AMSR-E. Journal of The Remote Sensing Society of Japan 29, 253–262.

Ma, Y., Wang, Y., Wu, R., Hu, Z., Yang, K., Li, M., Ma, W., Zhong, L., Sun, F., Chen, X., Zhu, Z., Wang, S., Ishikawa, H., 2009. Recent advances on the study of atmosphere-land interaction observations on the Tibetan Plateau. Hydrology and Earth System Sciences 13 (7), 1103–1111.

Njoku, E.G., Entekhabi, D., 1996. Passive microwave remote sensing of soil moisture. Journal of Hydrology 184, 101–129.

Njoku, E.G., Jackson, T.J., Lakshmi, V., Chan, T.K., Nghiem, S.V., 2003. Soil moisture retrieval from AMSR-E. IEEE Transactions on Geoscience and Remote Sensing 41, 215–229.

Pal, J.S., Eltahir, E.A.B., 2002. Teleconnections of soil moisture and rainfall during the 1993 Midwest summer flood. Geophysical Research Letters 29 (18), 1865, doi:10.1029/2002GL014815.

Paloscia, S., Macelloni, G., Santi, E., 2006. Soil moisture estimates from AMSR-E brightness temperatures by using a dual-frequency algorithm. IEEE Transactions on Geoscience and Remote Sensing 44, 3135–3144.

Pathmathevan, M., Koike, T., Li, X., 2003. A new satellite-based data assimilation algorithm to determine spatial and temporal variations of soil moisture and temperature profiles. Journal of Meteorological Society of Japan 81, 1111–1135.

Prigent, C., Aires, F., Rossow, W.B., Robock, A., 2005. Sensitivity of satellite microwave and infrared observations to soil moisture at a global scale: Relationship of satellite observations to in situ soil moisture measurements. Journal of Geophysical Research 110, D07110, doi:10.1029/2004JD005087.

Reichle, R.H., Mclaughlin, D.B., Entekhabi, D., 2001. Variational data assimilation of microwave radiobrightness observations for land surface hydrology applications. IEEE Transactions on Geoscience and Remote Sensing 39, 1708–1718.

Reichle, R.H., McLaughlin, D.B., Entekhabi, D., 2002. Hydrologic data assimilation with the ensemble Kalman filter. Monthly Weather Review 130, 103–114.

Reichle, R.H., Koster, R.D., 2005. Global assimilation of satellite surface soil moisture retrievals into the NASA catchment land surface model. Geophysics Research Letters 32, L02404, doi:10.1029/2004GL021700.

Reichle, R.H., Koster, R.D., Liu, P., Mahanama, S.P.P., Njoku, E.G., Owe, M., 2007. Comparison and assimilation of global soil moisture retrievals from the Advanced Microwave Scanning Radiometer for the Earth Observing System (AMSR-E) and the Scanning Multichannel Microwave Radiometer (SMMR). Journal of Geophysical Research 112, D09108, doi:10.1029/2006JD008033.

Sato, N., Sellers, P.J., Randall, D.A., Schneider, E.K., Shukla, J., Hou, Y.T., Albertazzi, E.R., 1989. Effects of implementing the simple biosphere model (SiB) in a GCM. Journal of the Atmospheric Science 46 (8), 2582–2757.

Sellers, P.J., Sud, Y.C., Dalcher, A., 1986. A simple biosphere model (SiB) for use within generation circulation models. Journal of the Atmospheric Science 43, 505–531.

Sellers, P.J., Los, S.O., Tucker, C.J., Justice, C.O., Dazlich, D.A., Collatz, G.J., Randall, D.A., 1996. A revised land surface parameterization (SiB2) for atmospheric GCMs. Part II: The generation of global fields of terrestrial biophysical parameters from satellite data. Journal of Climate 9 (4), 706–737.

Ulaby, F.T., Moore, R.K., Fung, A.K., 1986. Microwave Remote Sensing: Active and Passive. Artech House, Norwood, MA.

Van Den Hurk, B.J.J.M., 2002. European LDAS established. Gewex Newsletter 12 (2), 9.

Wagner, W., Scipal, K., Pathe, C., Gerten, D., Lucht, W., Rudolf, B., 2003. Evaluation of the agreement between the first global remotely sensed soil moisture data with model and precipitation data. Journal of Geophysical Research 108 (D19), 4611, doi:10.1029/2003JD003663.

Walker, J.P., Houser, P.R., 2001. A methodology for initializing soil moisture in a global climate model: Assimilation of near-surface soil moisture observations. Journal of Geophysical Research 106 (D11), 11761–11774.

Watanabe, T., Kondo, J., 1990. The influence of canopy structure and density upon the mixing length within and above vegetation. Journal of Meteorological Society of Japan 68, 227–235.

Xu, X.D., Lu, C.G., Shi, X.H., Gao, S.T., 2008a. World water tower: an atmospheric perspective. Geophysical Research Letters 35 (20), doi:10.1029/2008GL035867.

Xu, X.D., Zhang, R.H., Koike, T., Lu, C., Shi, X., Zhang, S., Bian, L., Cheng, X., Li, P., Ding, G., 2008b. A new integrated observational system over the Tibetan Plateau. Bulletin of the American Meteorological Society 89 (10), 1492–1496.

Yanai, C.J.P., Wu, C.G.X., 2006. Effect of the Tibetan Plateau. In: Wang, B. (Ed.), The Asian Monsoon. Springer, pp. 513–549.

Yanai, M., Song, Z., 1992. Seasonal heating of the Tibetan Plateau and its effects on the evolution of the Asian summer monsoon. Journal of the Meteorological Society of Japan 70, 319–351.

Yang, K., Koike, T., Fujii, H., Tamagawa, T., Hirose, N., 2002. Improvement of surface flux with a turbulence-related length. The Quarterly Journal of The Royal Meteorological Society 128, 2073–2087.

Yang, K., Watanabe, T., Koike, T., 2007. Auto-calibration system developed to assimilate AMSR-E data into a land surface model for estimating soil moisture and the surface energy budget. Journal of the Meteorological Society of Japan 85A, 229–242.

Yang, K., Chen, Y.-Y., Qin, J., 2009. Some practical notes on the land surface modeling in the Tibetan Plateau. Hydrology and Earth System Sciences 13, 687–701, doi:10.5194/hess-13-687-2009.

Ye, D.Z., 1981. Some characteristics of the summer circulation over the Qinghai-Xizang (Tibet) Plateau and its neighborhood. Bulletin of the American Meteorological Society 62, 14–19.

Ye, D.Z., Gao, Y., 1979. The Meteorology of the Qinghai-Xizang (Tibet), Plateau. Science Press, Beijing.

Ye, D.Z., Wu, G.X., 1998. The role of the heat source of the Tibetan Plateau in the general circulation. Meteorology and Atmospheric Physics 67, 181–198.